Characterising implicit LES methods

A. J. Aspden[1,2], N. Nikiforakis[2], S. B. Dalziel[2], and J. B. Bell[1]

[1]Lawrence Berkeley National Laboratory, 1 Cyclotron Road, MS 50A-1148, Berkeley, CA 94720, USA.

[2]Department of Applied Mathematics and Theoretical Physics, University of Cambridge, CB3 0WA, UK.

Abstract

Implicit LES methods employ high-order finite-volume schemes to capture the inviscid cascade of kinetic energy through the inertial range, and the inherent numerical error acts as an implicit subgrid model, forming a natural form of LES. However, the absence of a physical viscosity prohibits conventional characterisation of these methods, specifically how kinetic energy is dissipated at the grid scale and how to define a relevant Reynolds number. Kolmogorov's 1941 papers achieve this characterisation for real-world viscous fluids in terms of a universal equilibrium range determined uniquely by the rate of energy dissipation and the physical viscosity. Analogously, this paper proposes than an implicit LES method results in behaviour that can be characterised by a universal equilibrium range determined uniquely by the energy dissipation rate and the computational cell width. Implicit LES simulations of maintained homogeneous isotropic turbulence and of the Taylor-Green vortex are presented to support this proposal and highlight similarities and differences with real-world viscous fluids. Direct comparison with data from high resolution DNS calculations provides a basis for deriving an effective viscosity and an effective Kolmogorov length scale.

1 Introduction

The broad range of time and length scales present in high Reynolds number turbulent flows is often prohibitively expensive for direct numerical simulations to capture completely, and various techniques are used to attempt to circumvent this issue. An approach that is receiving increasing attention is to use a form of large eddy simulation (LES) known as implicit LES (ILES), where carefully constructed numerical schemes are used such that the inviscid energy

cascade is captured accurately and the inherent numerical error emulates the physical effects of the dynamics at the grid-scale cut-off. The philosophy of this approach was introduced by Boris *et. al.* [4], and referred to as Monotone Integrated Large Eddy Simulation (MILES), but has more recently come to encompass a broader range of schemes under the umbrella of ILES. In general, previous works have concentrated on how a particular scheme captures the inertial subrange of the kinetic energy spectrum, or have given an analytical assessment of the modified equations of motion. However, an issue that has not been satisfactorily addressed is that in the absence of a physical viscosity, it is not clear how to characterise a particular flow, e.g. how to define a Reynolds number; a property that is based on physical viscosity, and not necessarily one that should extend to an ILES calculation. In spite of this issue, this paper proposes a method for characterising ILES calculations, and then for relating the flow to a corresponding real-world viscous fluid in terms of an effective Kolmogorov length scale and an effective viscosity. An ILES scheme is used to evaluate these proposals and highlight conceptual similarities and differences between simulated and real-world viscous fluids.

Since turbulence is characterised by high levels of fluctuating vorticity and, therefore, sharp velocity gradients similar to compressible shocks, ILES is motivated by the principles behind shock-capturing schemes used for compressible flows. Specifically, high-order, non-oscillatory, finite-volume schemes are particularly well-suited to resolving these features. In the early 90's, several authors published successful applications of these types of schemes, e.g. Bell and Marcus [3], Porter *et. al.* [20] and Youngs [27], but it was Boris [4] who first identified the "convenient conspiracy", as it was later dubbed by Oran and Boris [19], specifically that the numerical error inherent in these schemes acts at the small scales in a similar manner to a subgrid-scale model. Furthermore, the cell-averaging discretisation of the flow variables can be thought of as an implicit filter. Therefore, these components combine to form a natural form of LES, and hence the name ILES.

Fureby and Grinstein [8] and Margolin and Rider [16] explored the implicit subgrid-scale models analytically (see also Grinstein and Fureby [11]), and it was demonstrated by Ghosal [10] that the numerical error in LES codes can be of a similar order of magnitude to the SGS model, and mask its effect. It was also shown by Fureby *et. al.* [9] and Menon *et. al.* [18] that in certain flows the

gross-scale features appear to be insensitive to the choice of SGS model, particularly if the spatial resolution is high enough. Using a PPM-based method, Sytine *et. al.* [24] and Porter *et. al.* [21] showed that it is possible to recover energy spectra with a minus five-thirds decay. Particular success has been found in free shear flows, where the influence of small-scale viscous dissipation is small, e.g. Aspden [2], and Fureby and Grinstein [8], and further applications and a more extensive discussion of the history of the approach can be found in Grinstein and Fureby [12], Drikakis *et. al.* [6], and Margolin *et. al.* [17].

The rest of the paper is organised as follows. In section 2, basic analysis analogous to Kolmogorov's 1941 papers [15] is presented, which is then investigated in section 3 by simulating two types of flow: maintained homogeneous isotropic turbulence and decaying turbulence in the context of the Taylor-Green vortex. Finally, the results are discussed in section 4.

2 Theory

An incompressible viscous flow has essentially three parameters, the integral length scale l, the energy dissipation rate ε, and the fluid viscosity ν. With two units of measure (length and time) dimensional analysis prescribes that the flow has a single dimensionless parameter, the Reynolds number

$$\mathrm{Re}_\varepsilon \equiv \frac{\varepsilon^{\frac{1}{3}} l^{\frac{4}{3}}}{\nu}.$$

This definition of the Reynolds number is proportional to the conventional Reynolds number defined using velocity instead of the dissipation rate; ε is used here for contextual convenience for turbulence discussions.

The conventional description of turbulence involves a cascade of kinetic energy from large to small scales where the energy is dissipated by viscosity. It is assumed that the Reynolds number is sufficiently large for a separation of scales to exist. Kolmogorov's first similarity hypothesis states that at scales $r \ll l$, the turbulent statistics are of a universal form, determined uniquely by the energy dissipation rate and the viscosity. This range of scales is known as the universal equilibrium range. Furthermore, Kolmogorov's second similarity hypothesis states that for scales

$\eta \ll r \ll l$, where

$$\eta \equiv \left(\frac{\nu^3}{\varepsilon}\right)^{\frac{1}{4}} \tag{1}$$

is the Kolmogorov length scale, the statistics are independent of viscosity and so are determined uniquely by the energy dissipation rate. This range of scales is known as the inertial (sub)range. The range of scales comparable with the Kolmogorov length scales, where kinetic energy is dissipated, is known as the dissipation (sub)range.

A key concept is that the energy dissipation rate is independent of the fluid viscosity, and moreover is determined solely by the large scales, i.e. by geometry or any forcing within the flow. For a particular fluid, the response to a varying energy dissipation rate is a change in the Kolmogorov length scale; viscosity essentially determines the length scale at which the energy is dissipated. Therefore, it should be expected that the large scales and inertial range should be the same in an ILES simulation as in a DNS simulation; only the dissipation range should be expected to differ.

Deriving the kinetic energy equation from the Navier-Stokes equations, the energy dissipation rate, averaged over a volume V, is found to be of the form

$$\varepsilon = \nu\mathcal{D}, \quad \text{where} \quad \mathcal{D} = \frac{1}{V}\int \mathbf{u}\cdot\nabla^2\mathbf{u}\,\mathrm{d}V; \tag{2}$$

$\mathcal{D}$ reflects the magnitude of velocity gradients that can be supported within the fluid.

Simple dimensional analysis can be employed to write an expression for the kinetic energy wavenumber spectrum in the universal equilibrium range,

$$E(\kappa) = \varepsilon^{\frac{2}{3}}\kappa^{-\frac{5}{3}}\varphi_\nu(\kappa\eta),$$

where κ is the magnitude of the wavenumber, and φ_ν is a (universal) dimensionless function. In the inertial range, independence from viscosity implies that φ_ν must be independent of its parameter, and must therefore be a (universal) constant, usually written C_κ, known as the Kolmogorov constant. In the dissipation range, φ_ν has been observed to decay exponentially, both in large-scale experiments by Saddoughi and Veeravalli [22] and in the DNS calculations by Kerr [14].

A similar approach can be taken to characterise an ILES scheme, but the resulting behaviour will differ from a real viscous fluid, and so will be referred to as an ILES fluid. Here, the parameters that describe the flow are l, ε and Δx (instead of ν). Dimensional analysis again prescribes a single dimensionless parameter $N = l/\Delta x$, which is crucially independent of ε. Only a change in resolution can result in a change in behaviour. This issue is how the resolution relates to the Reynolds number.

To draw the analogy with Kolmogorov's theory, it is first necessary to assume that the resolution is sufficiently high. Kolmogorov's first similarity hypothesis can then be restated such that for scales $r \ll l$, the turbulent statistics are of universal form determined uniquely by ε and Δx. The second similarity hypothesis remains unchanged, apart from the range of scales is $\Delta x \ll r \ll l$. As before, simple dimensional analysis can be employed to write an expression for the kinetic energy spectrum in this alternative universal equilibrium range

$$E(\kappa) = \varepsilon^{\frac{2}{3}} \kappa^{-\frac{5}{3}} \varphi_i(\kappa \Delta x).$$

In the inertial range, φ_i must be independent of Δx, and so again must be a constant. Importantly, independence from the details of small-scale energy dissipation suggests that this constant must be the same as in the viscous case, namely the Kolmogorov constant C_κ; energy from the large scales is advected inviscidly through the inertial range in the same way in an ILES calculation as in a real-world viscous fluid or DNS calculation.

To relate an ILES calculation to a viscous flow, simple dimensional analysis and empirical observations can be used to determine relationships between the parameters available from an ILES calculation, ε and Δx, and those from a viscous calculation, ε and ν. Specifically, expressions for an effective Kolmogorov length scale η_e and an effective viscosity ν_e can be derived in terms of Δx and ε. However, this set of parameters is incomplete. There are five parameters, l, ε, Δx, ν_e and η_e. The first of the three independent dimensionless quantities has be identified, N. The remaining two can be written as $\varepsilon \eta_e^4 / \nu_e^3$ and $\eta_e / \Delta x$. For consistency with viscous fluids, the former can taken to be unity; it simply forms a relationship between the two notional measures ν_e and η_e. The latter needs to be determined empirically, and moreover will be scheme-dependent. However, it is not clear how to define either η_e or ν_e in order to make the measurement. Therefore, an incompleteness arises because there is only one measurable

quantity that has units involving time. Another measurable quantity must be introduced to be able to relate an ILES fluid to a viscous fluid.

This new quantity should provide the link between the ILES and viscous fluids, specifically, the relation between Δx and ν, and so should be a common measure to both types of fluid. Also, it should reflect the effects of small scale energy dissipation. However, there is no reason to assume that the dissipation range in an ILES calculation should be structurally similar to that in a viscous flow; only the inertial range should be similar. For example, the smallest length scale in the inertial range does not depend strongly on the structure of the dissipation range, but is a consequence of viscous dissipation. Since kinetic energy is dissipated due to the numerical error inherent in the scheme when approximating (velocity) gradients, a measure of the gradients that are present in a flow is a reasonable choice for the new measure. To mimic the relationship with a viscous fluid, $\mathcal{D}$ can be taken as such a measure. Furthermore, the wavenumber spectrum of $\mathcal{D}$ will be structurally similar to $\kappa^2 E(\kappa)$, where E is the kinetic energy spectrum as a function wavenumber magnitude κ. Therefore, $\mathcal{D}$ will grow with $\kappa^{1/3}$ in the inertial range, and decay exponentially in the dissipation range. Hence, the largest contribution to the integral will come from length scales around the transition between the inertial and dissipation ranges, and not depend strongly on the structure of the dissipation range.

With this choice, dimensional analysis suggests that

$$\Pi_i \equiv \frac{\varepsilon^{\frac{1}{2}}}{\Delta x \mathcal{D}^{\frac{3}{4}}}$$

will be a universal constant for a given numerical scheme. In a viscous fluid,

$$\Pi_\nu \equiv \frac{\varepsilon^{\frac{1}{2}}}{\eta \mathcal{D}^{\frac{3}{4}}} \equiv 1,$$

and so provides a link between the two types of simulation; an effective Kolmogorov length scale can be defined as

$$\eta_e = \Pi_i \Delta x, \tag{3}$$

where Π_i is measured empirically. This choice for η_e with the relation $\nu_e \equiv \varepsilon^{1/3} \eta_e^{4/3}$ builds in the relation $\varepsilon = \nu_e \mathcal{D}$. The effective viscosity ν_e can then be written in terms of Δx using (3) as

$$\nu_e = \varepsilon^{\frac{1}{3}} \Pi_i^{\frac{4}{3}} \Delta x^{\frac{4}{3}},$$

highlighting some fundamental differences between a real-world viscous fluid and an ILES fluid, which will be discussed in detail below.

3 Simulations

The numerical code that is used throughout this study is IAMR, which was written at the Center for Computational Sciences and Engineering at the Lawrence Berkeley National Laboratory. It is an incompressible, variable-density Navier-Stokes solver that is capable of ILES calculations. A finite-volume approach is taken with a two-step predictor-corrector method. The flow variables are advected by a specialised upwind method before an approximate projection is used to enforced the divergence-free constraint. The method is second-order accurate in space and time. Details of the algorithm can be found in Almgren *et. al.* [1] and the references therein.

The equations of motion are the standard incompressible Navier-Stokes equations,

$$\begin{aligned} \nabla \cdot \mathbf{u} &= 0, \\ \frac{\partial \mathbf{u}}{\partial t} + (\mathbf{u} \cdot \nabla)\,\mathbf{u} &= -\frac{1}{\rho}\nabla p + \nu \nabla^2 \mathbf{u} + \mathbf{F}, \end{aligned}$$

where the density, velocity, pressure and viscosity are denoted by ρ, $\mathbf{u}$, p and ν, respectively, and $\mathbf{F}$ is a forcing term to be defined. The viscosity is simply set to zero for ILES calculations.

3.1 Maintained Homogeneous Isotopic Turbulence

Simulations were run of homogeneous isotropic turbulence in a triply-periodic unit cube[1]. To reduce the detrimental impact of long-range correlations that affect decaying turbulence, a time-dependent low-wavenumber forcing term was prescribed as

$$\mathbf{F}(\mathbf{x},t) = \sum_{|\boldsymbol{\kappa}|\in[1,3]} \mathbf{a}_{i,j,k} \cos(f_{i,j,k}t + \psi_{i,j,k}) \cos(2\pi\kappa_i x + p_{i,j,k}) \cos(2\pi\kappa_j y + q_{i,j,k}) \cos(2\pi\kappa_k z + r_{i,j,k}),$$

for random amplitudes $\mathbf{a}_{i,j,k} \in [0,1)$, frequencies $f_{i,j,k} \in [\pi, 2\pi)$, and phases $\psi_{i,j,k}$, $p_{i,j,k}$, $q_{i,j,k}$ and $r_{i,j,k} \in [0, 2\pi)$. The flow was initiated with a low-level low-wavenumber velocity field, and unit density.

[1] Throughout this section, the units are arbitrary, and Reynolds numbers will be presented where appropriate.

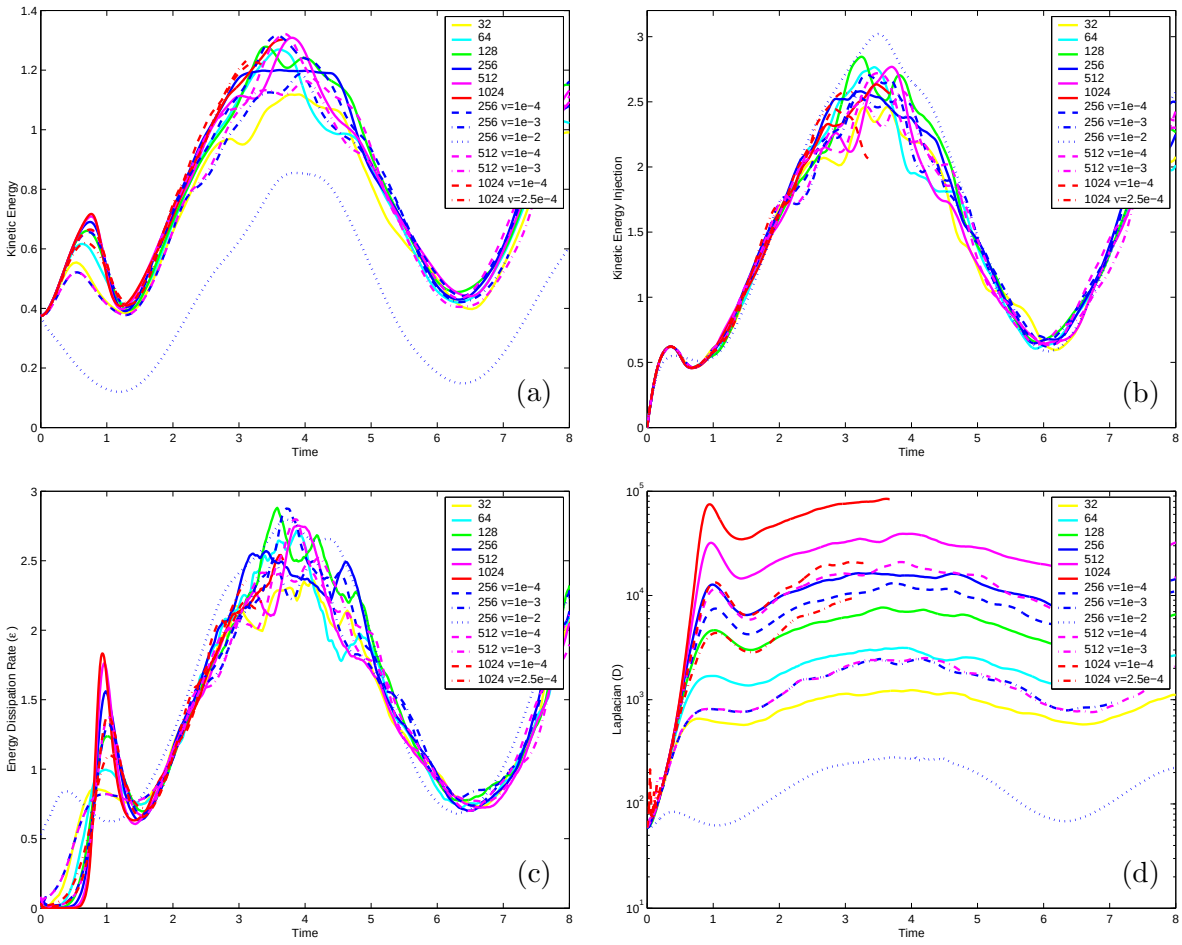

Figure 1: Evolution of (a) total kinetic energy E, (b) injection of kinetic energy due to the forcing term ϕ, (c) energy dissipation rate ε, and (d) the Laplacian term $\mathcal{D}$. Inviscid and viscous simulations are denoted by solid and broken lines, respectively, and colour denotes resolution.

Inviscid (ILES) simulations were performed at resolutions from 32^3 to 1024^3. Viscous simulations were performed at 256^3 (with viscosities of $\nu = 10^{-2}$, 10^{-3} and 10^{-4}), 512^3 (with viscosities of 10^{-3} and 10^{-4}) and at 1024^3 (with viscosities of 2.5×10^{-4}, and 10^{-4}). Not all of the viscous simulations were expected to be fully-resolved; evaluating Π_ν provides a way to establish which simulations are well-resolved and which are not. Simulations were run until $t = 8$, except for the 1024^3 cases, which were run until times between 3 and 4 due to computational expense.

Figures 1(a-d) show the evolution of the terms in the kinetic energy equation for all of the simulations; (a) is the total kinetic energy, (b) is the energy injected by the forcing term, (c) is the actual energy dissipation evaluated according to $\varepsilon = \phi - \mathrm{d}E/\mathrm{d}t$, where $\phi = (1/V) \int \mathbf{u} \cdot \mathbf{F} \, \mathrm{d}V$,

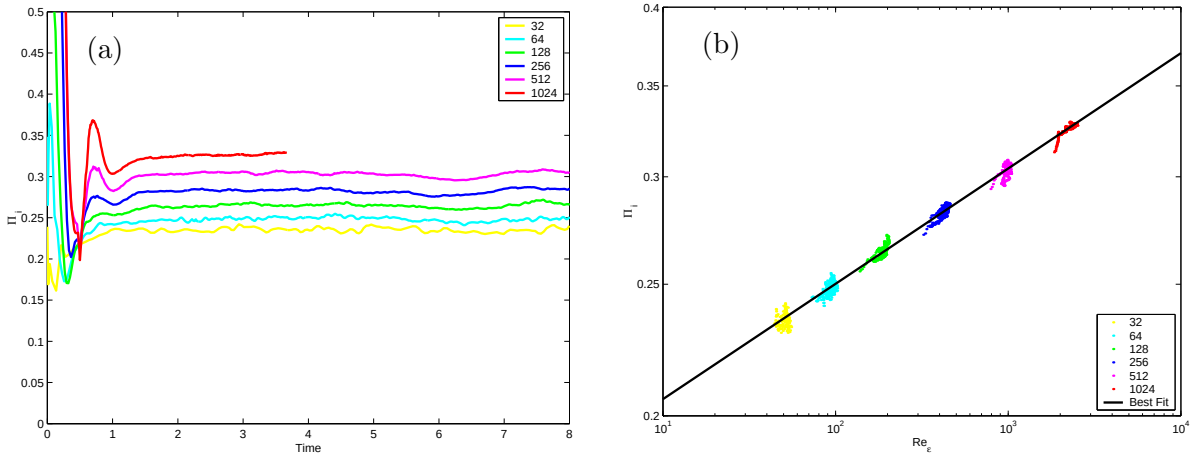

Figure 2: (a) Evolution of the dimensionless quantity Π_i for the ILES simulations. (b) Reynolds number dependence of Π_i. Data shown are for $t > 1.2$. The best fit is $\Pi_i = 0.169\mathrm{Re}_\varepsilon^{0.085}$.

and (d) is $\mathcal{D}$ as defined in (2). Inviscid and viscous runs are denoted by solid and broken lines, respectively, and colour denotes resolution. The flow passes through an initial transient as the energy cascade begins, the dissipation rate reaches a peak at around $t \approx 1$, and shortly thereafter becomes fully-developed. It is clear from these plots that the forcing term dominates the flow, but importantly maintains a time-dependent dissipation rate that is independent of the resolution and viscosity. Figure 1 demonstrates that the resolution and viscosity affect only the small-scale energy dissipation; it is only the Laplacian term $\mathcal{D}$ in figure 1(d) that is affected by changes in resolution or viscosity. In the most viscous case, the Reynolds number is too low for a sufficient separation of scales, and both the initial transient and the late-time evolution are heavily damped.

Figure 2(a) shows the evolution of the dimensionless quantity Π_i for the ILES simulations. For the resolutions presented here, the effective Kolmogorov length scale, defined in (3), is between about one quarter and one third of a computational cell width, which is much smaller than would be required for a well-resolved DNS calculation.

In each simulation, the value of Π_i becomes approximately constant once the flow has become well-developed, but there is a slight dependency on the resolution. In the dimensional analysis presented above, Reynolds number dependence was discounted relying on Kolmogorov's first similarity hypothesis. Figure 2(b) considers the dependence of Π_i on the effective Reynolds

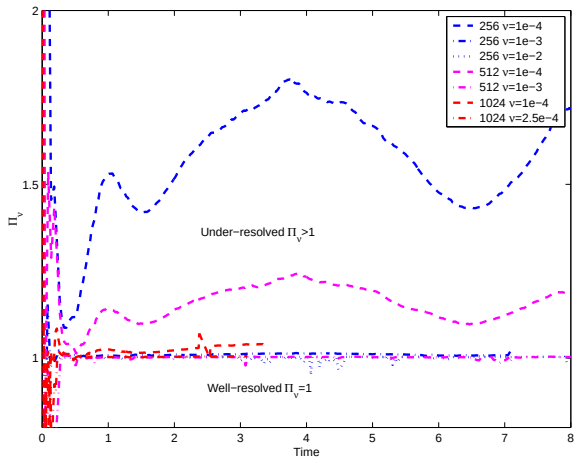

Figure 3: Evolution of the dimensionless quantity Π_ν. $\Pi_\nu \approx 1$ corresponds to a well-resolved viscous calculation, and $\Pi_\nu > 1$ denotes lack of resolution.

number, which has been defined as (2) but using the measured effective viscosity. The solid black line is a best fit to the power law $\Pi_i = 0.169\mathrm{Re}_\varepsilon^{0.085}$, demonstrating that there is in fact a very weak dependence of Π_i on the Reynolds number. Since the Reynolds number can be written as $\mathrm{Re} \equiv \Pi_i^{-4/3} N^{4/3}$, the expression for Π_i can be stated equivalently in terms of resolution as $\Pi_i = 0.203 N^{0.102}$, where N is the number of cells across the integral length scale.

The source of this dependency is not clear, but two possible influences have been discounted: the numerical slope limiting used to preserve monotonicity, and the use of a large scale forcing term. The simulations were run without utilising slope limiting, but this only resulted in a slightly smaller values for Π_i, the Reynolds number dependency remained. The decaying simulations in the next section will also be shown to possess a similar degree of dependency, discounting the forcing term.

It may be the case that the Reynolds number dependency is just a manifestation of an underlying limitation in relating an ILES simulation to a viscous fluid, which may be related to some other property of turbulence not considered here, such as intermittency. Recently, Sreenivasan [23] has argued that the resolution requirements for well-resolved DNS calculations grow at a rate that exceeds the three-quarters that natural scaling suggests, which may be related to the observations presented here.

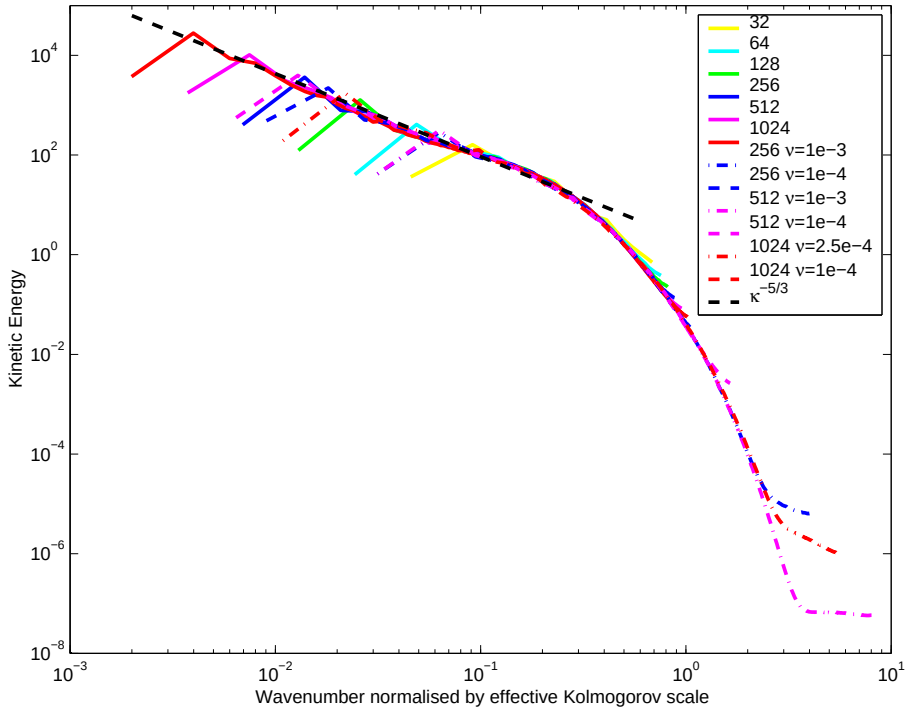

Figure 4: Normalised kinetic energy wavenumber spectra, $\varepsilon^{-2/3}\eta^{-5/3}E(\kappa\eta)$.

The measure Π_ν, shown in figure 3, distinguishes the viscous simulations that are well-resolved ($\Pi_\nu \approx 1$) from those that are not ($\Pi_\nu > 1$). The simulations at 256^3 with $\nu = 10^{-2}$, 512^3 with $\nu = 10^{-3}$ and 1024^3 with $\nu = 2.5 \times 10^{-4}$ are thought to be well-resolved as the maxima in Π_ν after the initial transient are 1.0052, 1.0045, and 1.0054, respectively (some error is expected due to evaluating the numerical derivatives for the temporal change in the total kinetic energy and the Laplacian). The simulations at 256^3 with $\nu = 10^{-3}$ and 1024^3 with $\nu = 10^{-4}$ are close, but not quite fully-resolved, where the maxima in Π_ν are 1.0145 and 1.0295, respectively. The other two simulations at $\nu = 10^{-4}$ are clearly not well-resolved.

Using the measured effective Kolmogorov length scales, the kinetic energy spectra can be normalised according to $\varepsilon^{-2/3}\eta^{-5/3}E(\kappa\eta)$, and are plotted in figure 4; the low Reynolds number DNS simulation has been omitted. The same colour scheme as before has been used, and the dashed black line shows the theoretical inertial range decay $C_\kappa\kappa^{-5/3}$ with a Kolmogorov constant of $C_\kappa = 2$. Even though ILES spectra are not expected to be identical to the viscous spectra, this normalisation appears to collapse both kinds of spectra in the universal equilibrium range; not only do the ILES spectra collapse to a single profile, that profile does not appear to be too far

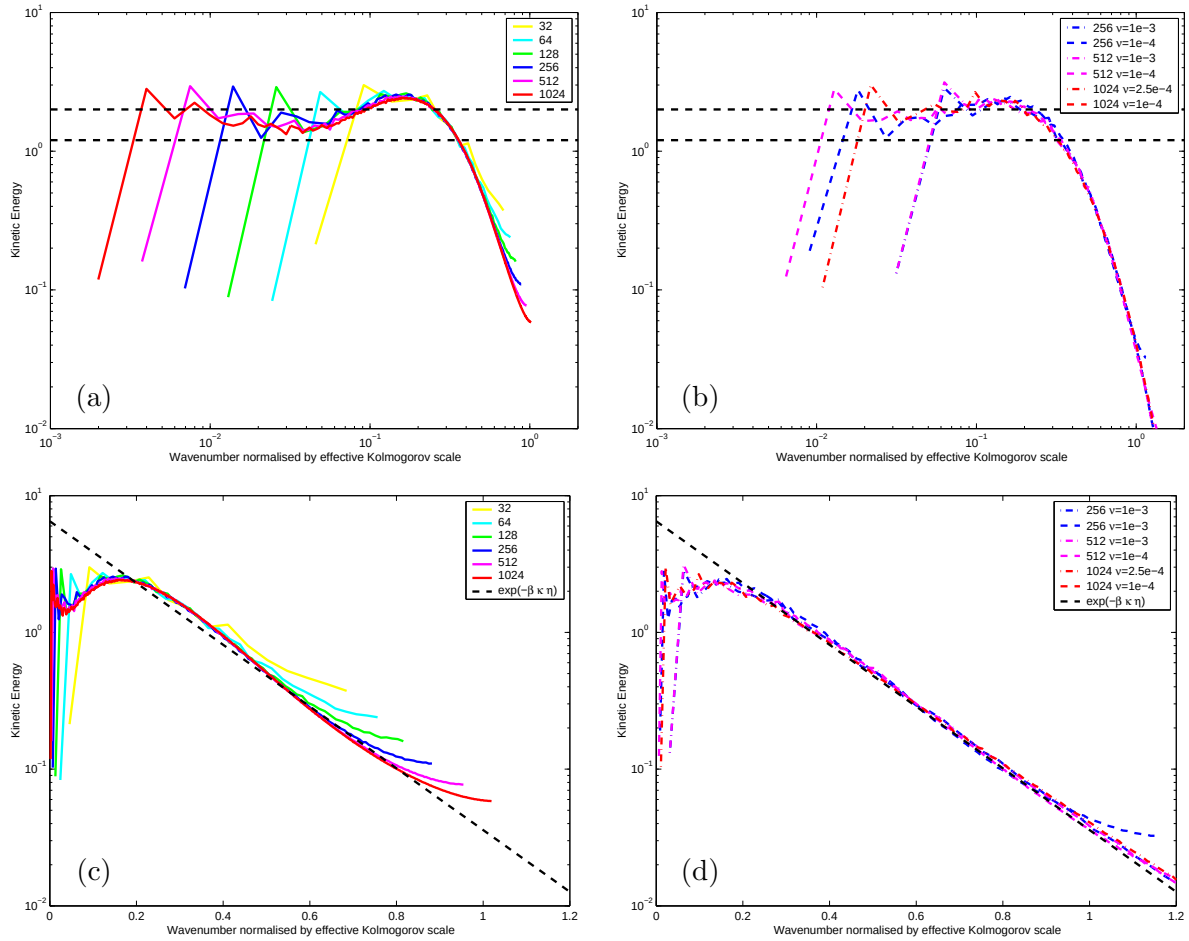

Figure 5: Compensated kinetic energy wavenumber spectra, normalised according to $\varepsilon^{-2/3}\kappa^{5/3}E(\kappa\eta)$. Inviscid spectra are shown in (a) and (c), and viscous spectra in (b) and (d). The inertial range is highlighted by logarithmic plots in (a) and (b) (the two black lines denote the range of values found in the literature for the Kolmogorov constant, i.e. 1.2 to 2), and the dissipation range is highlighted by semilogarithmic plots in (c) and (d).

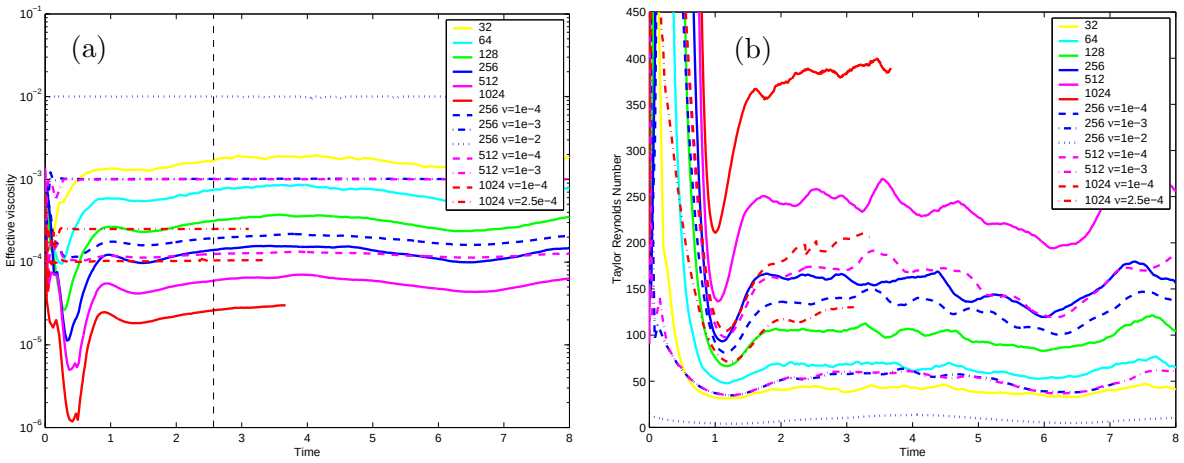

Figure 6: (a) Evolution of the effective viscosity ν_e, for both the inviscid and viscous simulations; note that the effective viscosity of the under-resolved viscous simulations does not agree with the specified viscosity. (b) Evolution of the Taylor Reynolds number.

removed from the viscous profile. In particular, it should be noted that the ILES spectra have a much shorter dissipation range compared with the viscous spectra; in the viscous simulations it is necessary to dedicate a significantly higher proportion of resolution to the dissipation range. Consequently, at the other end of the spectra, the ILES simulations have inertial ranges that extend to smaller wavenumbers than the viscous spectra, suggestive of higher Reynolds numbers. This behaviour can be seem more clearly in the compensated spectra, plotted in figure 5(a,b). Here, another difference between the two types of spectra can be discerned; the dip around $\kappa\eta \approx 0.05$ appears to be slightly greater in the ILES case. Figure 5(c,d) plots the compensated spectra semilogarithmically to consider exponential decay in the dissipation range. The dashed black line is $A\exp(-\beta\kappa\eta)$, with $A = 6.5$ and $\beta = 5.2$, taken from the DNS simulations of Kerr [14] and the boundary-layer experiments of Saddoughi and Veeravalli [22], with which the viscous simulations are in very close agreement. The ILES simulations, however, present slightly different behaviour; there is a range with steeper decay followed by a flattening near the grid-scale. In summary, there are identifiable differences between the equilibrium ranges of ILES and viscous spectra, but these differences are not sufficient to disrupt the collapse presented in figure 4, at least for the numerical scheme considered here. The scheme captures an inertial range close to the Kolmogorov constant, and the effective Kolmogorov length scale permits a normalisation that collapses the spectra to an equilibrium range that is universal for the scheme, and close to

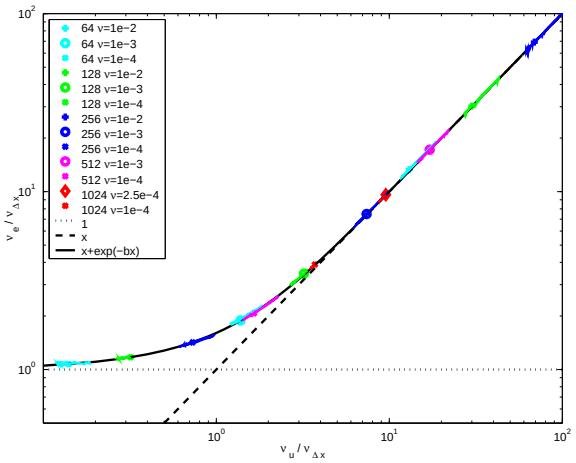

Figure 7: Examination of the dimensionless dependence of the effective viscosity on the specified viscosity in under-resolved viscous simulations, $\nu_e/\nu_{\Delta x} = f\left(\nu_u/\nu_{\Delta x}\right)$.

that of a real viscous fluid.

Figure 6(a) shows the evolution of the effective viscosity. The same measure is used in both the viscous and inviscid cases; the actual viscosity is not used explicitly, and so provides another measure of how well resolved the viscous calculations are. The vertical dashed line shows $t = 2.57$, which corresponds to the time at which the spectra are plotted in figures 4-5. A key point to note here is that the extent to which the inertial range of each spectrum extends to low wavenumbers (figure 4) corresponds directly to the effective viscosity at the time shown by the vertical dashed line (figure 6a). As Reynolds number increases, a larger inertial range is observed due to the greater separation of scales, so since all other quantities are approximately equal, the Reynolds number is represented by the effective viscosity, which follows exactly the same trend as the energy spectra at large scales. This suggests that the effective viscosity that has been derived is an accurate representation of the flow; if an ILES simulation and a viscous fluid have inertial ranges that extend over the same range of wavenumbers, then the method outlined above provides a way of deriving the effective viscosity of the ILES fluid corresponding to the true viscosity of the real fluid. The resulting effective Taylor Reynolds numbers are plotted in figure 6(b), where

$$\mathrm{Re}_\lambda = \frac{\hat{u}\lambda}{\nu_e} \quad \text{for} \quad \lambda^2 = \frac{15\nu_e\hat{u}^2}{\varepsilon},$$

where $\hat{u}$ is the RMS velocity.

To extend the characterisation to the situation of an under-resolved viscous calculation, there are three measures of viscosity that need to be considered; the specified (under-resolved) viscosity ν_u, the effective viscosity for an inviscid simulation at that resolution $\nu_{\Delta x}$, and the resulting effective viscosity ν_e. Dimensional considerations suggest a functional dependence of the form

$$\frac{\nu_e}{\nu_{\Delta x}} = f\left(\frac{\nu_u}{\nu_{\Delta x}}\right), \tag{4}$$

for some dimensionless function f, where $f(x) \to 1$ as $x \to 0$, and $f(x) \to x$ as $x \to \infty$.

To investigate this dependence, a variety of under-resolved simulations were run in addition to those already presented, the results of which are shown in figure 7. For each simulation, the marker denotes the time $t = 2.57$, and the surrounding points shows time dependence. The dotted line shows $f(x) = 1$ (the inviscid limit), the dashed line is $f(x) = x$ (the well-resolved viscous limit), and the solid black line is the heuristic candidate function

$$f(x) = x + \exp(-bx),$$

which naturally satisfies the restrictions on (4). The value of b shown here is $1/2$. There is clear agreement for all simulations, which suggests that an *a priori* prediction for the effective viscosity of an under-resolved viscous calculation using this scheme can be written as

$$\nu_e = \nu_u + \nu_{\Delta x} \exp\left(-\frac{1}{2}\frac{\nu_u}{\nu_{\Delta x}}\right).$$

3.2 The Taylor-Green Vortex

The Taylor-Green vortex [25] has become a popular test case for many advocates of ILES methods, see the recent studies of Drikakis *et. al.* [6] and Hickel *et. al.* [13], and so has been investigated here. Following [6], the domain used was a triply-periodic cube of length 2π. The velocity field was initialised according to

$$\mathbf{u}_0(\mathbf{x}) = u_0 \begin{pmatrix} \cos(kx)\sin(ky)\cos(kz) \\ -\sin(kx)\cos(ky)\cos(kz) \\ 0 \end{pmatrix},$$

where $k = 1$. The inherent symmetry of the problem can be exploited by using reflective boundary conditions to reduce the domain size by a factor of 8. Simulations were run at effective

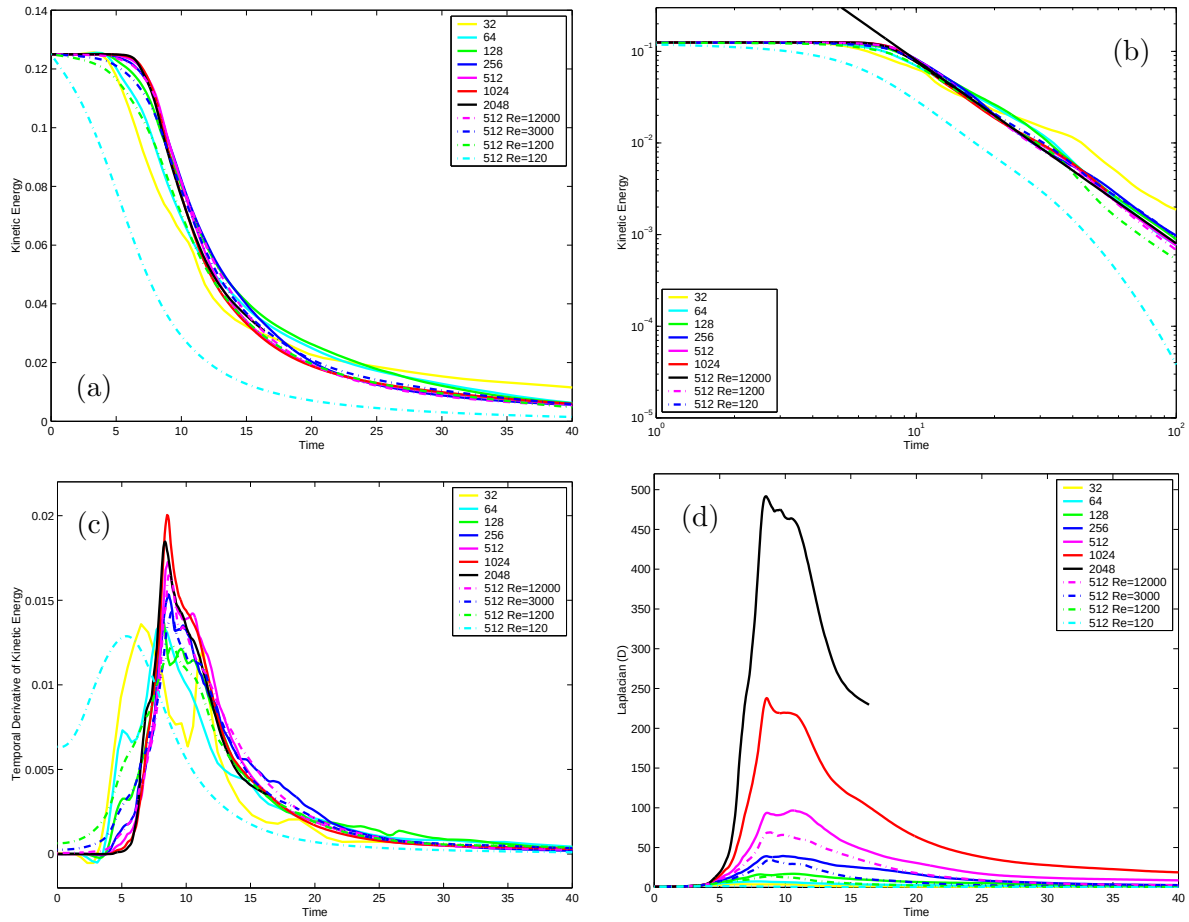

Figure 8: Evolution of the terms in the kinetic energy equation for the Taylor-Green vortex: (a,b) total kinetic energy, (c) temporal change in kinetic energy, (d) Laplacian term $\mathcal{D}$. The solid lines are the inviscid calculations and the dash-dotted lines are the viscous calculations.

resolutions of 32^3 to 2048^3. Viscous simulations were run at an effective resolution of 512^3, at Reynolds numbers of approximately 120, 1200, 3000, and 12000, where the Reynolds number is defined to be $\mathrm{Re} = u_0/k\nu$, corresponding to the initial conditions; as with the previous section, this range of Reynolds numbers span the range from under-resolved at this resolution to too viscous for a separation of scales. Throughout this section velocities will be non-dimensionalised by u_0 and lengths by k^{-1}.

Figure 8(a,b) show the evolution of the normalised total kinetic energy, (c) shows the temporal derivative of the kinetic energy, and (d) shows the Laplacian term $\mathcal{D}$. At early times, kinetic energy is conserved (in the inviscid and high Reynolds number cases), then as the cascade process begins, a growth in the Laplacian term is observed along with a corresponding decay in kinetic

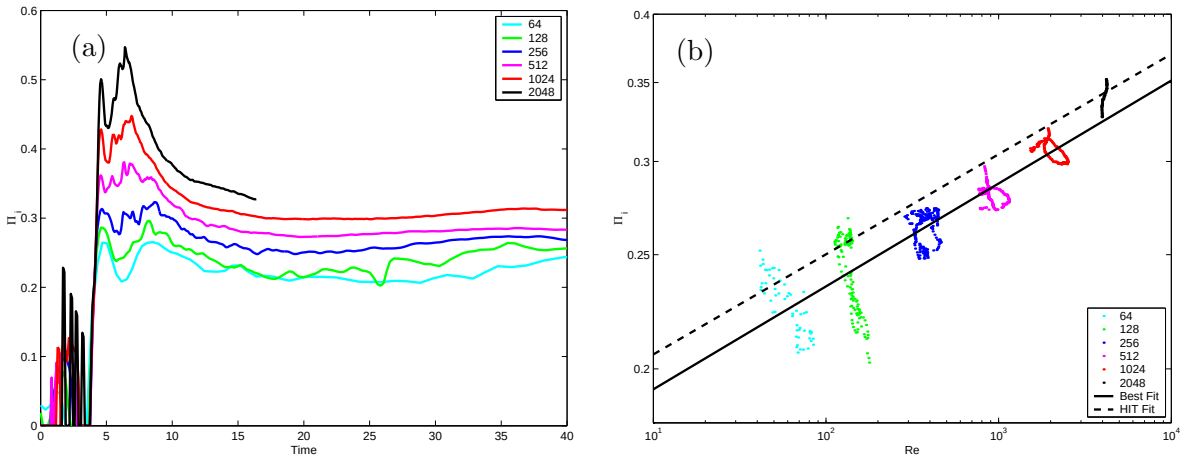

Figure 9: (a) Evolution of the dimensionless parameters Π_i. (b) Dependence of Π_i on Re_ε. Data shown are for $t > 12$. Solid black line denotes best fit, $\Pi_i = 0.152\mathrm{Re}_\varepsilon^{0.087}$. Dashed black line is the best fit from the previous section.

energy. The energy dissipation rate reaches a peak at around dimensionless time $t \approx 9$, and the late-time energy decay follows t^{-2}, characteristic of the Taylor-Green vortex. The most viscous case prevents transition to turbulence, and the vortex spins down at a rate that can be seen to be faster than t^{-2} at late times.

In the ILES results of Drikakis *et. al.* [6] and the DNS results of Brachet [5] at a Reynolds number of 5000, the energy dissipation is observed to peak at a value around 0.016, and it is suggested in Frisch [7], for example, that a limit independent of Reynolds number is being approached. However, the peak energy dissipation in the 1024^3 case presented in figure 8(c) is approximately 25% higher, and so suggests that much higher Reynolds numbers will be needed to draw any definitive conclusions. The simulation at 2048^3 does not attain a peak as high as the 1024^3 case. This is because the Taylor-Green vortex is extremely sensitive to shear instabilities, which are damped at lower resolutions.

Figure 9(a) shows the dimensionless quantity Π_i. There is a slightly greater variability in the value of Π_i for each simulation than there was for the simulations in the previous section, and again there is a dependence on resolution. Figure 9(b) shows the Reynolds number dependency of Π_i for each simulation. The solid black line denotes the best fit to the data, which is of the form $\Pi_i = 0.152\mathrm{Re}_\varepsilon^{0.087}$. The dashed black line shows the best fit from the simulations from the

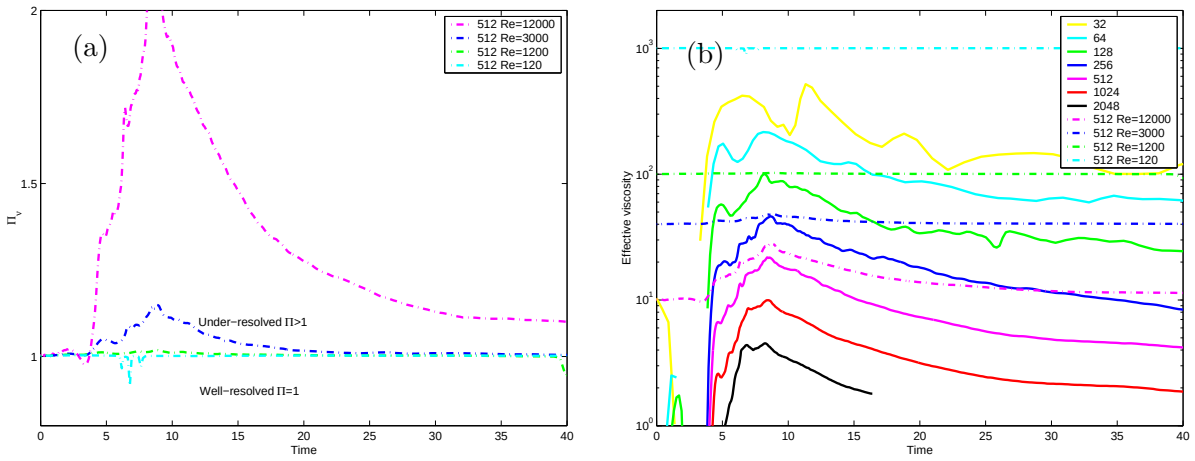

Figure 10: (a) Evolution of the dimensionless parameter Π_ν. (b) Evolution of the effective viscosity ν_e.

previous section, which has a similar power-law growth, but a slightly higher coefficient.

Figure 10 shows the dimensionless quantity Π_ν (a), and the effective viscosities (b). The least viscous case is clearly identified as being under-resolved, but because the flow is decaying, the simulation approaches the well-resolved limit at late times. The $\mathrm{Re} = 3000$ case appears to be marginally under-resolved, but the other two viscous cases appear to be well-resolved.

Figure 11 shows the kinetic energy spectra, normalised as before using the effective Kolmogorov length scale and energy dissipation rate, along with reference spectra from the maintained homogeneous isotropic turbulence simulations from the previous section, specifically the inviscid simulation at 1024^3 and the well-resolved viscous simulation at 512^3 with $\nu = 10^{-3}$; the dashed black line denotes $C_\kappa \kappa^{-5/3}$, with $C_\kappa = 2$. The low wavenumber peak is a signature of the Taylor-Green vortex, due to the initial conditions. Again, the normalisation collapses the data well, not only the viscous and inviscid simulations, but also the maintained and decaying flows; a universal equilibrium range is indeed recovered in these ILES simulations, and appears to be similar to that recovered in a viscous fluid.

Compensated spectra are shown in figures 12(a,b) for two different times: (a) is at $t \approx 16.4$, the latest time that the highest resolution case was run, and (b) is at $t \approx 50$. At the first time, the compensated spectra demonstrate that the decay is close to minus-five thirds, but the later time highlights one of the drawbacks of decaying turbulent simulations; without a source of energy

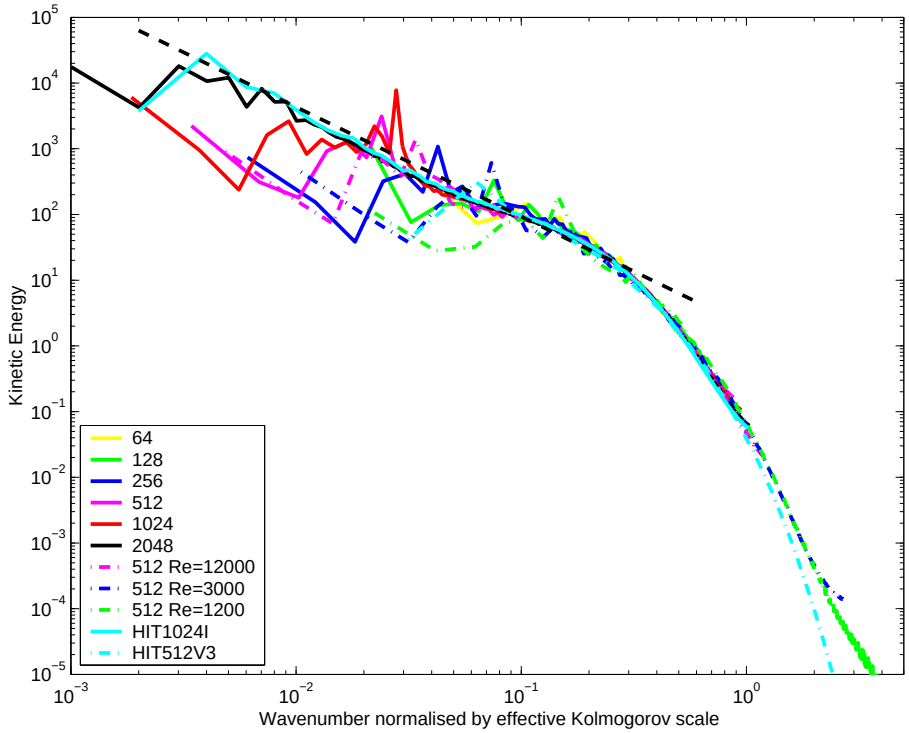

Figure 11: Kinetic energy wavenumber spectra, $\varepsilon^{-2/3}\eta^{-5/3}E(\kappa\eta)$, at dimensionless time $t \approx 2$. Two maintained simulations from the previous section (labelled HIT) are shown for comparison; specifically the inviscid simulation at 1024^3 and the viscous simulation at 512^3 with $\nu = 10^{-3}$.

at the large scales, the wavenumbers over which an inertial range can be observed is restricted and the decay with wavenumber is much smaller. The compensated spectra from the viscous calculations (not shown) are at Reynolds numbers too low to be able to observe an extensive inertial range.

A key difference between ILES simulations and real-world viscous or DNS fluids arises in flows that are decaying, and is due to the fixed effective Kolmogorov length scale in the ILES case. In a viscous fluid, as the flow decays, the energy dissipation rate drops, and so the Kolmogorov length scale increases according to (1). This cannot happen in an ILES fluid; instead, the effective viscosity decreases. The consequence of this is that all small-scale structure is removed from the viscous flow, but high-wavenumber velocity gradients persist in the ILES case. This is highlighted in figure 13, which shows a vertical slice of the magnitude of vorticity at $t = 100$ for both a viscous calculation (512^3, Re ≈ 3000) and an inviscid calculation (256^3); there is structure at

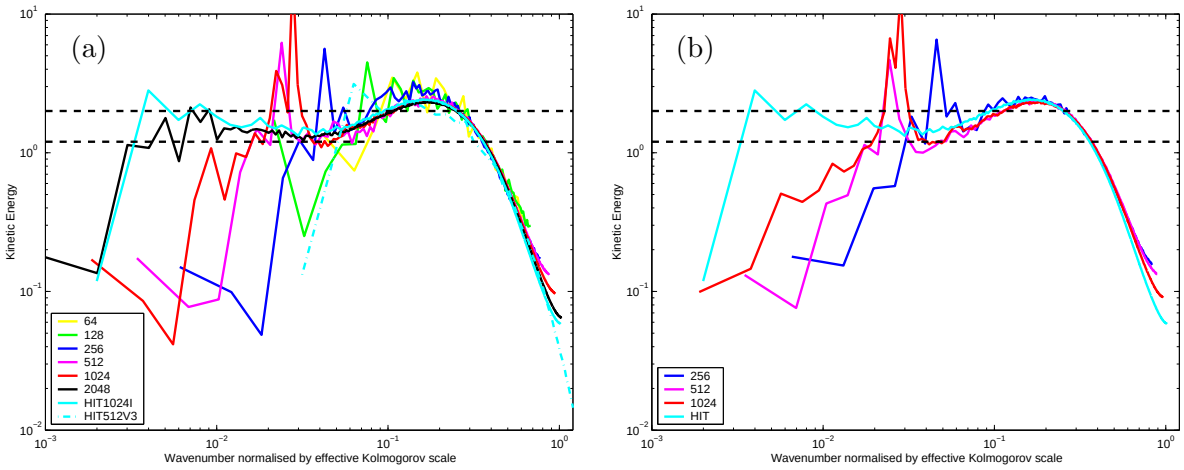

Figure 12: Compensated kinetic energy wavenumber spectra for the Taylor-Green vortex, normalised according to $\varepsilon^{-2/3}\kappa^{5/3}E(\kappa\eta)$. (a) $t \approx 16.4$, (b) $t \approx 50$.

shorter length scales in the inviscid calculation even at a lower resolution.

4 Discussion and Conclusions

In this paper, an approach has been presented for characterising implicit LES methods by drawing an analogy with the characterisation of viscous fluids following Kolmogorov [15]. Specifically, an ILES code can be characterised in terms of an equilibrium range that is universal to that code, and is determined uniquely by the energy dissipation rate ε, as in a viscous fluid, and the computational cell width Δx, which replaces the fluid viscosity as the characteristic measure of small-scale energy dissipation. Simple dimensional analysis was then employed, arriving at a dimensionless parameter that was empirically demonstrated to collapse for two quite different flows and across a substantial range of resolutions, albeit with a slight Reynolds number dependence. Specifically, it was found that $\Pi_i = 0.169\mathrm{Re}_\varepsilon^{0.085}$ or equivalently $\Pi_i = 0.203N^{0.102}$, where N is the number of computational cells across the integral length scale.

To mimic the relationships of viscous fluids, an effective Kolmogorov length scale and effective viscosity were then defined as $\eta_e = \Pi_i \Delta x$ and $\nu_e = \varepsilon^{1/3}{\Pi_i}^{4/3}\Delta x^{4/3}$, which means that the effective Kolmogorov length scales for the simulations presented here were between one quarter and one third of a computational cell width.

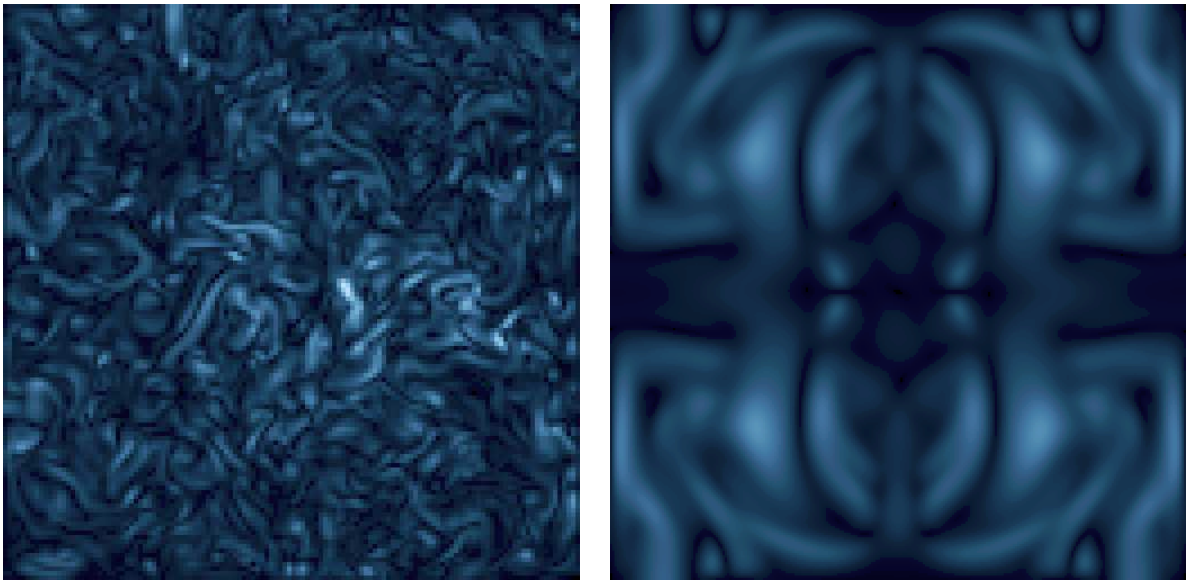

Figure 13: Vertical slice showing late-time magnitude of vorticity in an inviscid calculation (left) and in a viscous calculation (right). It is clear how small-scale structure is removed by viscosity, but persists in an ILES calculation due to the imposed separation of scales.

These measures were used to normalise kinetic energy spectra, and it was demonstrated, by comparison with well-resolved DNS calculations, that an ILES flow with an effective viscosity close to that of a DNS calculation had an inertial range that spanned the same range of wavenumbers; this measure of effective viscosity is an accurate representation of an ILES fluid.

Furthermore, under-resolved simulations were investigated, and it was found that a simple expression could be formulated to predict the effective viscosity *a priori*:

$$\nu_e = \nu_u + \nu_{\Delta x} \exp\left(-\frac{1}{2}\frac{\nu_u}{\nu_{\Delta x}}\right).$$

Differences were observed between ILES and viscous spectra, both at the high wavenumber end of the inertial range, and within the dissipation range. These differences were small however, and only observed under close scrutiny.

A key difference is that the effective viscosity depends on the energy dissipation rate, which is local in both time and space, and so knowledge of some kind of measure of the dissipation rate (in whatever average sense applies to the flow) is required. This means that not only does the effective viscosity vary in time, but can be different at different points in the flow, and even both.

In a turbulent jet, for example, a higher effective viscosity will be observed along the jet axis than at the jet edge because of the decreasing dissipation rate with radius, see Townsend [26] for example. Furthermore, the Reynolds number will increase with streamwise distance, rather than remain constant as expected in a round jet. In decaying flows, a significant consequence is that the ILES flow cannot undergo relaminarisation; there is no final period of decay. In a decaying viscous flow, as the energy dissipation rate drops, the Kolmogorov length scale increases as small-scale structure is removed by viscosity. This cannot happen in an ILES fluid; there is an imposed separation of scales due to the fixed Kolmogorov length scale. The vorticity field will decay, but cannot become smooth; small-scale structure will persist for all time.

Attention should also be drawn to the fact that the expression for the effective viscosity can be rewritten in the form $\nu_e = \varepsilon/\mathcal{D}$, which has no *a priori* reason to hold true in an ILES flow. It may be the case that because the scheme is second-order accurate (Margolin *et. al.* [17] argue that second-order may be the only suitable way to construct an ILES scheme), then $\mathcal{D}$ is indeed a close measure of how energy is removed from the system. Moreover, the wavenumber spectrum for $\mathcal{D}$ will be similar to $\kappa^2 E(\kappa)$, which suggests that the dominant contribution to the integral is from length scales at the transition between the inertial and dissipation subranges, which lies within the resolved scales of the ILES simulations presented above, and the spectra are observed to be close those of the viscous calculations. Furthermore, the contribution to the integral is not dominated by the dissipation scales, which will be scheme-dependent.

This raises the question of how different ILES implementations will compare with the results presented here: should different ILES codes produce results that are structurally similar to those presented here? The parameter Π_i is the dimensionally correct scaling to characterise a scheme, but its value (and any Reynolds number dependence) will vary between different implementations. For example, it is expected that higher-order schemes will present spectra that have a compensated spectrum with the peak energy at the bottleneck between the inertial and dissipation ranges that is greater and at a higher normalised wavenumber compared to those found here. It may also be observed that the dip in the spectra observed at wavenumbers smaller than this peak will also be exaggerated. It is anticipated that such schemes will have smaller values for Π_i.

It has been demonstrated, both here and by many previous authors, that ILES methods provide an effective approach for simulating high Reynolds number turbulent flows, particularly in regimes where there is a large-scale source of energy that is driving the system (e.g. free shear or gravitationally driven flows) and where the specific details of energy dissipation (e.g. Prandtl or Schmidt number effects, or late-time decay) are not the primary concern. Differences between ILES and real-world viscous fluids have been highlighted, but in spite of these differences a method has been proposed that gives the best characterisation to date of an ILES fluid, as an entity in its own right, and in the context of a viscous fluid.

Acknowledgements

AJA's time at DAMTP was funded by an AWE/EPSRC CASE award, and at LBNL by a Seaborg Fellowship. JBB was supported by the Office of Advanced Scientific Computing Research, Applied Mathematics Research Program of the U.S. Department of Energy under Contract No. DE-AC02-05CH11231. Calculations have been performed on Franklin at NERSC, Atlas at LLNL, Jaguar at NCCS, Blue Oak at AWE and Franklin at the Cambridge-Cranfield HPCF. AJA would also like to thank David Youngs, Robin Williams, Colm Caulfield and Malcolm Andrews for their useful discussions.

References

[1] A. S. Almgren, J. B. Bell, P. Colella, L. H. Howell, and M. L. Welcome. A Conservative Adaptive Projection Method for the Variable Density Incompressible Navier-Stokes Equations. *Journal of Computational Physics*, 142(1):1–46, 1998.

[2] A. J. Aspden. Monotone integrated large eddy simulation of buoyant turbulent jets with off-source heating. *PhD Thesis, University of Cambridge*, 2006.

[3] J. B. Bell and D. L. Marcus. Vorticity Intensification and Transition to Turbulence in the Three-Dimensional Euler Equation. *Communications in Mathematical Physics*, 147, 1992.

[4] J. P. Boris, F. F. Grinstein, E. S. Oran, and R. L. Kolbe. New insights into large eddy simulation. *Fluid Dynamics Research*, 10:199–229, 1992.

[5] M. E. Brachet. Direct simulation of three-dimensional turbulence in the Taylor-Green vortex. *Fluid Dynamics Research*, 8:1–8, 1992.

[6] D. Drikakis, C. Fureby, F. F. Grinstein, and D. L. Youngs. Simulation of transition and turbulence decay in the Taylor-Green vortex. *Journal of Turbulence*, 8:1–12, June 2004.

[7] U. Frisch. *Turbulence. The legacy of A.N. Kolmogorov*. Cambridge University Press, 1995.

[8] C. Fureby and F. F. Grinstein. Monotonically Integrated Large Eddy Simulation of Free Shear Flows. *AIAA Journal*, 37:544–556, 1999.

[9] C. Fureby, G. Tabor, H. G. Weller, and A. D. Gosman. Differential subgrid stress models in large eddy simulations. *Physics of Fluids*, 9:3578–3580, November 1997.

[10] S. Ghosal. An Analysis of Numerical Errors in Large-Eddy Simulations of Turbulence. *Journal of Computational Physics*, 125:187–206, April 1996.

[11] F. F. Grinstein and C. Fureby. Recent Progress on MILES for High Reynolds Number Flows. *Journal of Fluids Engineering*, 124:848–861, December 2002.

[12] F. F. Grinstein and C. Fureby. From canonical to complex flows: Recent progress on monotonically integrated LES. *Computing in Science and Engineering*, 6:37–49, 2004.

[13] S. Hickel, N. A. Adams, and J. A. Domaradzki. An adaptive local deconvolution method for implicit LES. *Journal of Computational Physics*, 213:413–436, 2006.

[14] R. M. Kerr. Velocity, scalar and transfer spectra in numerial turbulence. *Journal of Fluid Mechanics*, 211:309–332, 1990.

[15] A. N. Kolmogorov. (a) The local structure of turbulence in incompressible viscous fluid for very large Reynolds numbers, and (b) Dissipation of Energy in the Locally Isotropic Turbulence. *Royal Society of London Proceedings Series A*, 434:(a) 9–13, and (b) 15–17, July 1991.

[16] L. G. Margolin and W. J. Rider. A rationale for implicit turbulence modelling. *International Journal for Numerical Methods in Fluids*, 39:821–841, 2002.

[17] L. G. Margolin, W. J. Rider, and F. F. Grinstein. Modeling turbulent flow with implicit LES. *Journal of Turbulence*, 7:1–27, January 2006.

[18] S. Menon, P.-K. Yeung, and W.-W. Kim. Effect of subgrid models on the computed interscale energy transfer in isotropic turbulence. *Computers and Fluids*, 25:165–180, February 1996.

[19] E. S. Oran and J. P. Boris. Computing Turbulent Shear Flows - A Convenient Conspiracy. *Computers in Physics*, 7:523, 1993.

[20] D. H. Porter, A. Pouquet, and P. R. Woodward. Three-dimensional supersonic homogeneous turbulence: A numerical study. *Phys. Rev. Lett.*, 68:3156, 1992.

[21] D. H. Porter, A. Pouquet, and P. R. Woodward. Kolmogorov-like spectra in decaying three-dimensional supersonic flows. *Physics of Fluids*, 6:2133–2142, June 1994.

[22] S. G. Saddoughi and S. V. Veeravalli. Local isotropy in turbulent boundary layers at high Reynolds number. *Journal of Fluid Mechanics*, 268:333–372, 1994.

[23] K. R. Sreenivasan. Resolution effects in direct numerical simulations of turbulence. In *Turbulent Mixing and Beyond Workshop, Trieste, Italy*, July 2007.

[24] I. V. Sytine, D. H. Porter, P. R. Woodward, S. W. Hodson, and K.-H. Winkler. Convergence tests for the piecewise parabolic method and Navier-Stokes solutions for homogeneous compressible turbulence. *Journal of Computational Physics*, 158:225–238, 2000.

[25] G. I. Taylor and A. E. Green. Mechanism of the Production of Small Eddies from Large Ones. *Proceedings of the Royal Society of London, Series A*, 158:499–521, February 1937.

[26] A. A. Townsend. *The Structure of Turbulent Shear Flow.* Cambridge University Press, 1967.

[27] D. L. Youngs. Three-dimensional numerical simulation fo turbulent mixing by Rayleigh-Taylor instability. *Physics of Fluids A*, 4:1312–20, 1991.